Available online at www.sciencedirect.com
ScienceDirect
Journal of the European Ceramic Society 31 (2011) 2447–2451
www.elsevier.com/locate/jeurceramsoc

Morphological and phase control of tin oxide single-crystals synthesized by dissolution and recrystallization of bulk SnO powders

Sheng-Chang Wang [a,*], Ray-Kuang Chiang [b,*], Pin-Jie Hu [a]

[a] Department of Mechanical Engineering, Southern Taiwan University, Yungkang City, Tainan 710, Taiwan, ROC
[b] Department Materials Science and Engineering, Far East University, Tainan 744, Taiwan, ROC

Available online 27 March 2011

Abstract

Various types of tin oxide particle, including square SnO platelets, truncated octahedral SnO crystals, and monodispepersed SnO_2 nanoparticles, were synthesized by the dissolution and recrystallization of bulk SnO powder via the thermal decomposition of tin oleate in a coordinating solvent of tri-n-octylamine at 340 °C. The results reveal that the atmosphere and reaction time are important factors that affect the shape of tin(II) oxide and the oxidation state of tin(II or IV) oxide. As tin oleate decomposed in a N_2 atmosphere, truncated octahedral SnO crystals formed. When the thermal decomposition was conducted in air, square SnO platelets formed after a 30-min reaction time. When the reaction time was extended to 180 min, the square SnO platelets decomposed and transformed into nanocrystalline SnO_2 particles.

Keywords: Powders-chemical preparation; Grain growth; Electron microscopy; Grain size; Sensors

1. Introduction

Nanostructured metal oxide and semiconductor materials are highly desirable for advanced electronic, magnetic, optoelectronic and sensing applications.[1,2] The performance of nanoparticles strongly depends on their phase, size, shape, and dimension. Hence, the control of these properties is of great interest.

Tin oxides, such as tetragonal SnO and rutile-type SnO_2, have received a lot of attention as functional materials. SnO is used in p-type semiconductors, high-energy-density rechargeable lithium batteries,[3,4] and solar energy storage.[5] SnO_2 is widely used for various devices, such as transparent conductive electrodes,[6] gas sensors,[7,8] electrochromic devices,[9] and anodes for batteries.[10,11] A lot of effort has thus been devoted to the synthesis of SnO and SnO_2 nanoparticles and nanostructured materials. Moreover, SnO is a versatile intermediate to metallic Sn, Sn_3O_4, and SnO_2.[12] However, the steady growth of single-crystal SnO is relatively difficult because Sn(II) is not a thermodynamically stable phase and is easily oxidized to Sn(IV) in the atmosphere.

Tin oxide nanostructures of various sizes, phases, and shapes have been prepared through various gas-phase and liquid-phase routes. Zero-dimensional nanoparticles,[13–17] one-dimensional nanowires,[7] nanorods,[18] and nanotubes, two-dimensional nanoplates,[19] nanoribbons,[1] and nanofilms,[13] and three-dimensional mesoporous structures[20,21] have been reported. However, the preparation methods generally involve the use of tin salts dissolved in aqueous or polar solvents. The present study reports that SnO can be easily dissolved in hot oleic acid and that the resulting tin(II) oleate complex can be used as an efficient precursor for the synthesis of nanoparticles of SnO and SnO_2. Furthermore, the shape of the obtained SnO single-crystals can be easily controlled by reaction atmospheres. Alternatively, the phase of tin oxides can be controlled by the reaction time.

2. Experimental details

Chemical oleic acid (OA, 90%, SHOWA, Japan) and commercial SnO powder (Riedel-de Haen, Germany) were used to form the tin oleate complex. Tri-n-octylamine (TOA, 90%, Kanto, Japan) was used as the coordinating solvent along with a phase transformation controller reagent.

The synthesis procedure was as follows. The precursor was synthesized using 1 mmol of SnO powder loaded in a 50-ml three-necked flask together with 2 mmol of OA. The mixture was

* Corresponding authors.
E-mail addresses: scwang@mail.stut.edu.tw (S.-C. Wang), rkc.chem@msa.hinet.net (R.-K. Chiang).

0955-2219/$ – see front matter © 2011 Elsevier Ltd. All rights reserved.
doi:10.1016/j.jeurceramsoc.2011.02.024

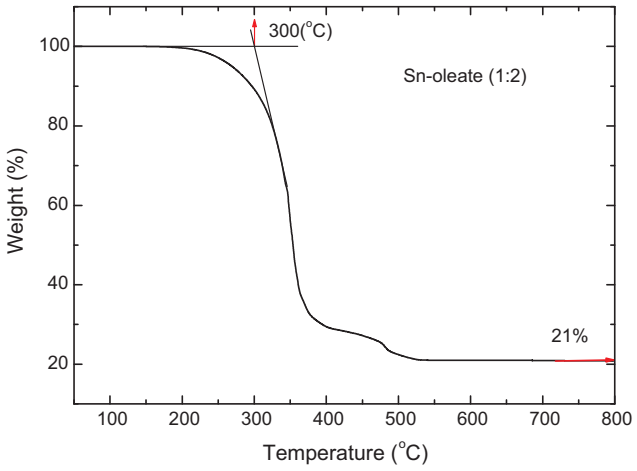

Fig. 1. Thermal gravimetric analysis of as-prepared precursor gel.

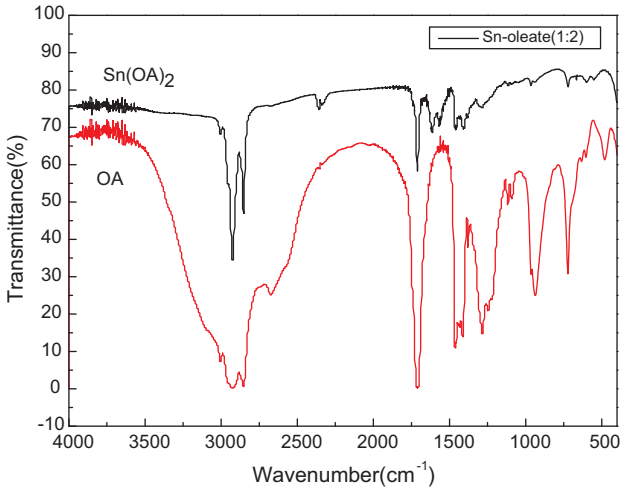

Fig. 2. FTIR spectra of (a) oleic acid and (b) the precursor gel.

stirred to obtain a clear solution, which was cooled to become the precursor gel.

The particles were synthesized via the re-dissolution of the precursor gel at 100 °C under a vacuum of ~1 mbar for 20 min. The reaction vessel was then filled with N_2 or air and the temperature was increased to 250 °C at a heating rate of 20 °C/min; this temperature was maintained for 20 min to give a clear solution. 4 ml of TOA was injected into the reaction vessel and heated and stirred at a temperature of 340 °C.

The precursor gel was characterized using a thermogravimetry (TGA, Pyris 1, Perkin Elmer, USA) and a Fourier transform infrared spectroscope (FTIR, Nicolet 5700, USA). The resulting suspensions were centrifuged, and the precipitate powder was thoroughly washed with acetone and redispersed in hexane. Crystalline phases of the powders were identified using X-ray diffractometry (XRD, Shimadzu 6000 Lab, Japan). The surface morphologies and dimensions of the products were examined using a scanning electron microscope (SEM, Hitachi S-3000N, Japan) and a field emission gun transmission electron microscope (FEG-TEM, FEI, TECNAI G2 F-20, Netherlands).

3. Results and discussion

3.1. Synthesis and characterization of tin oleate complex

Fig. 1 shows the TGA curve of a precursor gel prepared via the dissolution of SnO powder in hot oleic acid with a molar ratio of SnO to oleic acid of 1/2. According to the curve, the as-synthesized material starts to decompose at 200 °C and reaches a steady state at a temperature of 500 °C. The treated powder after an 800 °C reaction was identified as the SnO_2 phase from XRD pattern. The residual weight of the TGA curve for the complete reaction is about 21%. Compared with the molar fraction of the product SnO_2 (150.708 g/mol) and the starting tin oleate complex $Sn(C_{18}H_{35}COO)_2$ (685.648 g/mol) is 22%, which is very close to the residual weight from the TGA result.

Bonding analysis was also conducted. The FTIR spectra of the oleic acid and the precursor gel are shown in Fig. 2. Comparing the two spectra, a new peak at 1551 cm^{-1} was formed, which indicates that the C–O stretching of the as-formed tin carboxylate bond is more constrained than that of the free acids (1709 cm^{-1}). Thus, the SnO powder dissoluted in oleic acid and formed the tin oleate complex $Sn(C_{18}H_{35}COO)_2$ at 250 °C. The reaction can be written as:

$$2SnO + 2R\text{-}COOH \rightarrow (R\text{-}(COO))_2\text{-}Sn + H_2O$$

where R is $CH_3(CH_2)_7CH{=}CH(CH_2)_7$.

3.2. Synthesis of various types of tin oxide particles

In the thermal decomposition process, when TOA was injected into the clear tin oleate complex solution and heated to 340 °C in air, the color of the reaction mixture changed from clear to brown after 20 min, and then became white after a further 180 min. In the presence of a N_2 atmosphere, the color of the reaction mixture changed from clear to brown after a 20-min reaction and remained in the same color after a further 180 min reaction time. The change of color implies occurrence

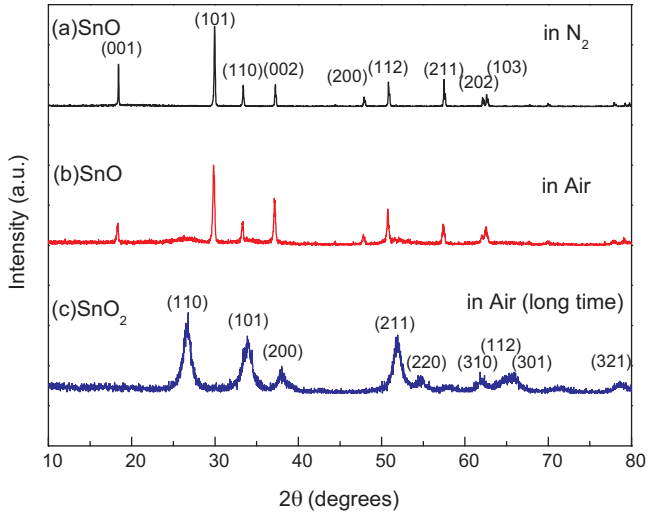

Fig. 3. XRD spectra of the (a) as-received powder prepared in N_2 atmosphere for 20 min, and (b) as-received powder prepared in air for 30 min and (c) for 3 h.

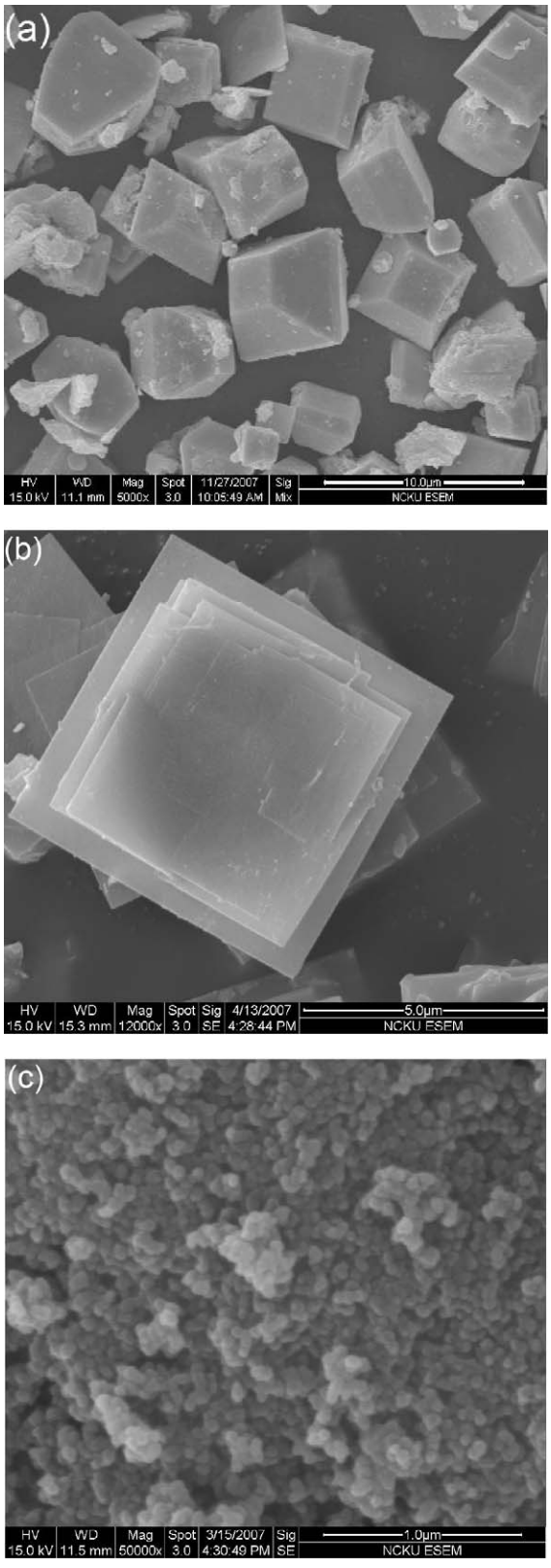

Fig. 4. SEM micrographs of (a) as-received powder prepared in N_2 atmosphere for 20 min, and (b) as-received powder prepared in air for 30 min and (c) for 3 h.

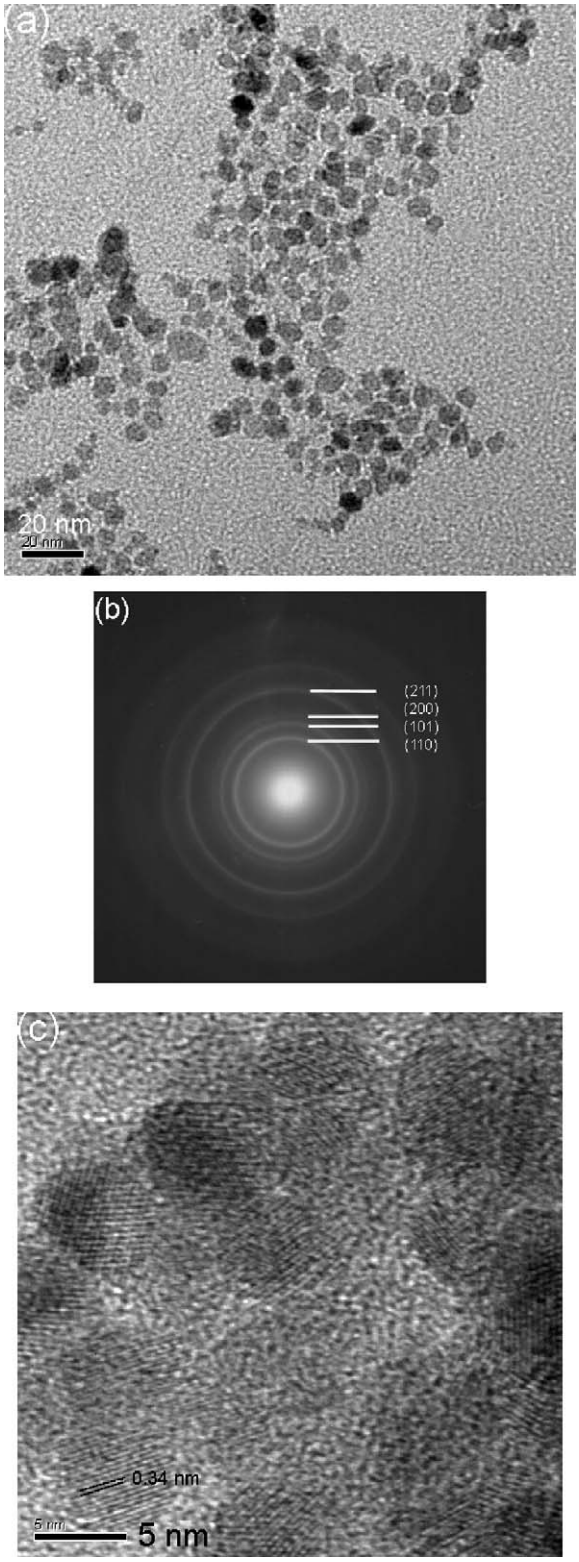

Fig. 5. (a) TEM micrographs of monodispersed SnO_2 nanoparticles, (b) SADP of nanoparticles in (a), and (c) HRTEM image of SnO_2 nanoparticles.

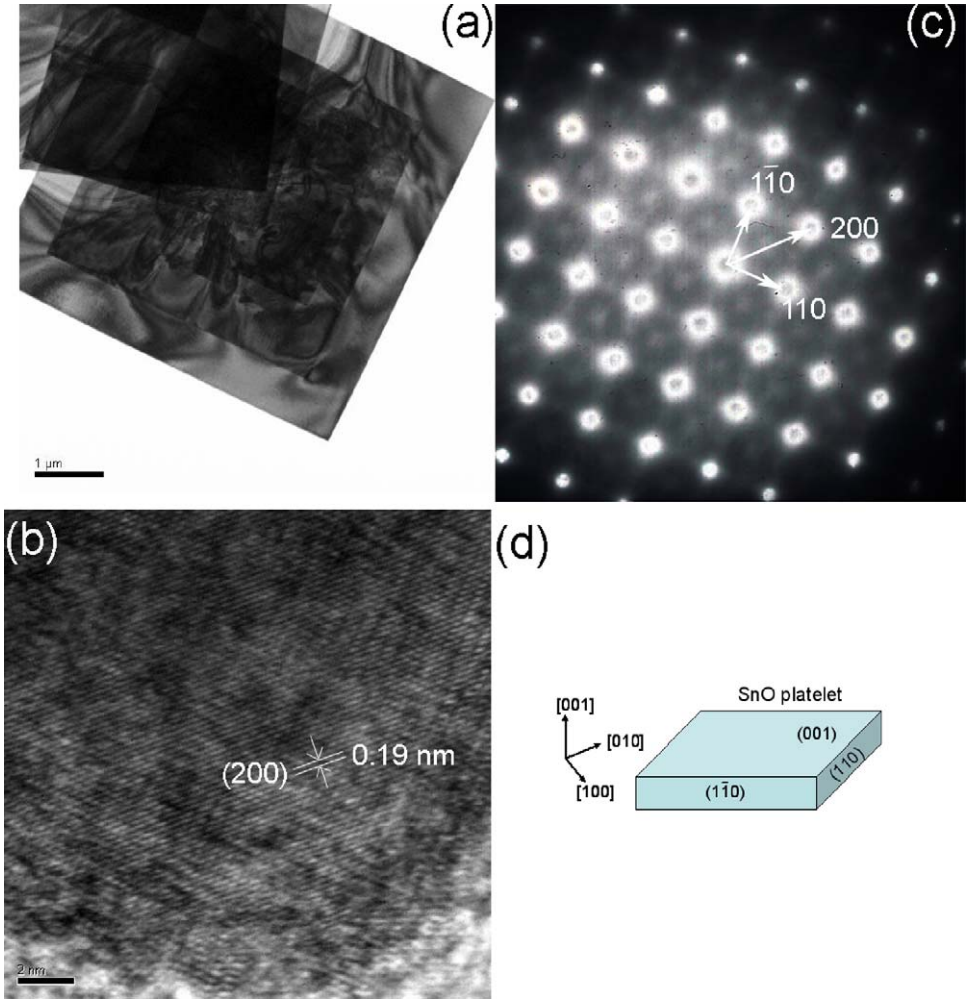

Fig. 6. (a) TEM micrograph of square SnO nanoplatelets, (b) HRTEM lattice image of square SnO nanoplatelets, (c) SADP of square SnO nanoplatelets, and (d) schematic geometrical shape and crystalline planes of square SnO nanoplatelets.

of precipitation or phase changed. Fig. 3 shows the powder XRD patterns of the products annealed in a N_2 atmosphere for 20 min, and in air for a short time (20 min) and a long time (3 h). When the thermal decomposition reaction was conducted in a N_2 atmosphere, the product exhibited the SnO phase (*P4/nmm*, $a = 3.802$ Å, $c = 4.836$ Å, JCPDS No. 06-0395). The sharp peaks indicate that the SnO is well crystalline and that the particle size is large. In addition, the diffraction intensities of the (0 0 1) and (0 0 2) planes have higher intensity ratios than those of the standard powder diffraction file, which implies that the powder has a long length in [0 0 1] direction. Moreover, when the thermal decomposition time was increased to 3 h, the reaction precipitation phase remained the SnO phase. When TOA was added into the tin oleate complex solution in air, the complex decomposed and formed tetragonal SnO crystals at 20 min. When the reaction time increased to 3 h, the SnO crystals oxidized further to the rutile SnO_2 phase ($P4_2/mnm$, $a = 4.7382$ Å, $c = 3.1871$ Å, JCPDS No. 41-1445). The broad peaks in the pattern indicate that the SnO_2 particles were in the form of a nanocrystalline powder. The particle size estimated using Scherrer's equation is about 7 nm.

The morphology and dimension of the products characterized by SEM are shown in Fig. 4. The two SnO crystals prepared under different atmospheres have distinctly different shapes and sizes. For SnO formation in N_2, the powder is in the form of decahedral crystals with perfect facets with a size of 4–5 μm, as shown in Fig. 4(a). However, the as-synthesized SnO platelet powder produced in air for 30 min is in the form of square disk-like crystals. The typical dimensions of the SnO platelets are 6 μm × 6 μm in square edge length and 100 nm in thickness (see Fig. 4(b)). When the synthesis time was longer than 3 h, the SnO platelet powder decomposed and transformed into SnO_2 nanosized powder, as shown in Fig. 4(c).

The SEM results show that the transformed SnO_2 particles are small, spherical, and monodispersed. Fig. 5(a) shows a TEM micrograph of the SnO_2 nanoparticles, which confirms that the size is uniform. The diffraction pattern of the powder (Fig. 5(b)) shows obvious ring patterns which are assigned to the (1 1 0), (1 0 1), (2 0 0), and (2 1 1) planes of the SnO_2 rutile structure. Fig. 5(c) shows high-resolution TEM micrographs of the SnO_2 nanoparticles, which exhibit a clear lattice fringe with a size of 6–7 nm and an interval of

0.34 nm, corresponding to the (1 1 0) lattice spacing of SnO_2 crystals.

Fig. 6(a) shows TEM micrographs of the square SnO nanoplatelets and corresponding high-resolution TEM image, which indicates that the SnO nanoplatelets were single-crystal. The SnO nanoplatelets are thin enough to be transparent for an electron beam. Some bending contours present obviously on the whole single crystal. Two or three smaller SnO platelets are well-stacked on the center of a large SnO nanoplatelet. The high-resolution image of the SnO edge indicates that the interlayer spacing is about 1.90 Å, attributed to the (2 0 0) plane of a romarchite SnO structure. The diffraction pattern in Fig. 6(c) shows a [0 0 1] zone pattern of tetragonal SnO crystals. From the TEM image and the diffraction pattern, it was determined that the square edge is {1 1 0} facets, and that the normal direction of the SnO platelet is [0 0 1]. A schematic geometrical shape and the crystalline planes of SnO platelets are shown in Fig. 6(d).

3.3. Growth mechanism

Base on experimental results, we propose a formation mechanism for tin oxide. The less stable SnO powder dissolved in the OA solvent and formed a tin oleate complex. When TOA was added into the tin oleate complex solution and heated to 340 °C, the tin oleate molecules decomposed into SnO monomers. The SnO monomers are very difficult to isolate in high temperature and recrystallization occur to growth as stable particle. The coordinating solvent TOA works as an activator that triggers the decomposition reaction as well as a surfactant that controls the shape of the SnO particles. The SnO monomers are like building blocks which assemble into SnO particles on a large scale to minimize the surface energy. According to Wang's[22] report, the shape of a tetragonal SnO single crystal is determined by the growth rates along the ⟨0 0 1⟩, ⟨1 0 0⟩, and ⟨1 1 0⟩ directions. When the thermal decomposition process was conducted in a N_2 atmosphere, the TOA surfactant was stable and adsorbed onto the surface of the SnO nuclei isotropically. The growth rates of the tetragonal SnO single crystal along the ⟨0 0 1⟩, ⟨1 0 0⟩, and ⟨1 1 0⟩ directions are equal, leading to a decahedral structure. However, the TOA molecules in air during the decomposition process is unstable and oxide to form cation radical, which selectively adsorbs onto the (0 0 1) plane of the SnO crystal and suppresses the growth rate of the (0 0 1) plane. Finally, the anisotropic assembled into a large square SnO sheet crystal.

4. Conclusions

Single-crystalline SnO in the forms of square nanoplatelets and a truncated octahedral shape was synthesized from the thermal decomposition of tin oleate precursor, prepared using commercial SnO powder dissolved in oleic acid. The morphology and oxidation state of tin oxide varied with atmosphere and reaction time of the decomposition process. Truncated octahedral and square nanoplatelets of SnO were selectively synthesized under air and nitrogen atmospheres, respectively. Nanocrystalline SnO_2 particles with a size of 6–7 nm formed after a prolonged decomposition time. The shape of SnO crystals is controlled by the TOA anisotropic adsorption behavior in N_2 or air. The air atmosphere tends to suppress the growth rate of SnO in the [0 0 1] direction, whereas N_2 leads to isotropic growth.

References

1. Pan ZW, Dai ZR, Wang ZL. *Science* 2001;**291**:1947.
2. Guo Y-G, Hu J-S, Wan L-J. *Adv Mater* 2008;**20**:2878–87.
3. Idota Y, Kubota T, Matsufuji A, Maekawa Y, Miyasaka T. *Science* 1997;**276**:1395.
4. Park MS, Wang GX, Kang YM, Wexler D, Dou SX, Liu HK. *Angew Chem Int Ed* 2007;**46**:750.
5. Ferrere S, Zaban A, Gregg BA. *J Phys Chem B* 1997;**101**:4490.
6. Cachet CH, Gamard A, Campet G, Jousseaume B, Toupance T. *Thin Solid Films* 2001;**388**:41.
7. Qin L, Xu J, Dong X, Pan Q, Cheng Z, Li F. *Nanotechnology* 2008;**19**:185705.
8. Li K-M, Li Y-J, Lu M-Y, Kuo C-I, Chen L-J. *Adv Funct Mater* 2009;**19**:2453–6.
9. Olivi P, Pereira EC, Longo E, Varella JA, Bulhoes LO. *J Electrochem Soc* 1993;**140**:L81.
10. Zhu J, Lu Z, Aruna ST, Aurbach D, Gedanken A. *Chem Mater* 2000;**12**:2557.
11. Aurbach D, Nimberger A, Markovsky B, Levi E, Sominski E, Gedanken A. *Chem Mater* 2002;**14**:4155–63.
12. Dai ZR, Pan ZW, Wang ZL. *J Am Chem Soc* 2002;**124**:8673.
13. Ba J, Polleux J, Antonietti M, Niederberger M. *Adv Mater* 2005;**17**:2509–12.
14. Leite ER, Maciel AP, Weber IT, Lisboa-Filho PN, Longo E, Paiva-Santos CO, et al. *Adv Mater* 2002;**14**:905.
15. Ribeiro C, Lee EJH, Giraldi TR, Longo E, Varela JA, Leite ER. *J Phys Chem B* 2004;**108**:15612–7.
16. Bose AC, Thangadurai P, Ramasmy S. *Mater Chem Phys* 2006;**95**:72–8.
17. Liang C, Shimizu Y, Sasaki T, Koshizaki N. *J Phys Chem B* 2003;**107**:9220–5.
18. Zanotti L, Zha M, Calestani D, Comini E, Sberveglieri G. *Cryst Res Technol* 2005;**40**:932–5.
19. Uchiyama H, Ohgi H, Imai H. *Cryst Growth Des* 2006;**6**:2188–90.
20. Ginley DS, Bright C. *MRS Bull* 2000;**25**:15.
21. Qi L, Ma J, Cheng H, Zhao Z. *Langmuir* 1998;**14**:2578–81.
22. Wang ZL. *J Phys Chem B* 2000;**104**:1153.